Fermi National Accelerator Laboratory

FERMILAB-Pub-96/394

Photon Emission from 511 KeV Gamma Rays Incident on BaF_2 and $LaF_3:Nd^{3+}$ Crystals Using a Cesium Iodide Photocathode Detector

W. Kononenko et al.

Fermi National Accelerator Laboratory
P.O. Box 500, Batavia, Illinois 60510

October 1996

Submitted to *Nuclear Instruments & Methods*

Operated by Universities Research Association Inc. under Contract No. DE-AC02-76CH03000 with the United States Department of Energy

Disclaimer

Distribution

Photon emission from 511 KeV gamma rays incident on BaF_2 and LaF_3:Nd^{3+} crystals using a cesium iodide photocathode detector

W. Kononenko, J. G. Heinrich, N. S. Lockyer and J. M. Miller
University of Pennsylvania, Philadelphia, PA 19104

C. Woody
Brookhaven National Laboratory
P. O. Box 5000, Upton, NY 11973-5000

S. Kwan
Fermi National Accelerator Laboratory
Batavia, IL 60510

Abstract

We have studied the possibility of using BaF_2 and LaF_3-doped with Nd^{3+} concentrations ranging from 0.1 to 15 mol% as efficient convertors of 511 KeV gamma rays. We have measured the number of photoelectrons/MeV for both crystals using a parallel-plate avalanche chamber operating with a CsI photocathode. The photocathode is sensitive to wavelengths in the range 160-220 nm. The fast component of the BaF_2 emission spectrum has peaks at roughly 175, 195 and 200 nm, and the LaF_3:Nd^{3+} emission spectrum peaks at 173 nm. We measure $3.71 \pm 0.04 \pm 1.11$ photoelectrons per MeV for the BaF_2 and $4.81 \pm 0.04 \pm 1.44$ photoelectrons per MeV for the LaF_3:Nd^{3+}. The results for BaF_2 and LaF_3:Nd^{3+} are consistent with estimates that are based on measured scintillation properties of these crystals.

1 Introduction

There is interest in growing crystals that convert gamma rays to visible or ultra-violet (UV) light. These crystals have applications in particle and nuclear physics, astronomy, as well as in medical imaging, such as in positron emission tomography (PET). More specifically, we have been intrigued with the possibility that a full-body-size detector sensitive to gamma rays could

be built inexpensively and be insensitive to magnetic fields. This type of detector has the potential to perform full-body PET scans and to be incorporated into a magnetic resonance imaging detector, thus allowing for simultaneous images of the anatomy and functionality without the need of computer merging techniques now employed.

The detector is a low-pressure parallel-plate avalanche chamber (PPAC) with a cesium iodide (CsI) photocathode for the detection of UV photons [1, 2]. The detector is sensitive to photon wavelengths between 160 and 220 nm, with a quantum efficiency of 22% at 170 nanometers [3]. The quantum efficiency falls with longer wavelengths. We have tested two crystals: barium fluoride (BaF_2) and lanthanum fluoride doped with Nd^{3+} concentrations ranging from 0.1 to 15 mol% (LaF_3:Nd^{3+}). Positrons are emitted from a Na^{22} source, which annihilate to produce two 511 KeV gamma rays. The crystals convert the incident 511 KeV gamma rays into UV photons, which are either lost or absorbed by the CsI photocathode. A resulting photoelectron is amplified in the gas and the signal is detected with a charge sensitive preamplifier. A final system would likely employ a wire-chamber with a CsI photocathode operated at atmospheric pressure [4].

This paper reports the first results from measuring the number of detected photoelectrons from a LaF_3:Nd^{3+} crystal using a PPAC and a CsI photocathode. A BaF_2 crystal is also tested and used for comparison. The results are consistent with Monte Carlo simulations that are based on measurements of the light yield by the DELFT group [5, 6, 7], but are lower than the yields reported in Ref. [8]

2 Detector

A schematic layout of the detector is shown in Fig. 1 and in Fig. 2. The detector is a low-pressure PPAC. It is built from a stainless steel vacuum vessel 20.3 cm in diameter and 4.4 cm thick with a removable 15.2 cm×1.27 cm thick quartz window. A pad plane, which is a double-sided printed circuit board with plated through holes, on standard FR-4 epoxy glass or ceramic material, is 10.2 cm in diameter by 1.6 mm thick. The pad plane has 84 pads 8×8 mm^2 with one central pad 16×16 mm^2. A 100 nm thick cesium iodide photocathode was evaporated in vacuum onto an aluminum substrate. A stainless steel mesh plane having 80% normal transmission is fixed at a

distance of 2 mm from the pad plane. The chamber was operated with 20 Torr of ethane gas and a high voltage of 520 volts was applied to the mesh for these tests. The UV light source was a hydrogen-discharge lamp coupled with a monochromator located 20 cm (air gap) from the window and was used for the single photoelectron calibration.

A 7.2 μCi Na^{22} source was used to provide two 511 KeV gamma rays per positron annihilation. A sodium iodide (NaI) crystal, 5 cm in diameter and 5 cm thick, mounted on a 5 cm diameter photomultiplier was used as a trigger. The threshold was set to select the 511 KeV gamma ray band, and a 6 μs gate was generated to reduce the number of out of time signals in the PPAC. The trigger rate was typically 2 kHz. The electrical signal induced on the central 13 pads (3.2$\times$ 3.2 cm^2 in area and electrically connected) was amplified and shaped (1 μs time constant) and sent to an EG&G analog-to-digital convertor connected to a personal computer.

The detector configurations are slightly different for the two crystals because the LaF_3:Nd^{3+} crystal is very small and could not easily be used as a replacement for the quartz window. The LaF_3:Nd^{3+} crystal is cylindrical in shape, 0.8 cm in diameter and 1.7 cm in length. It is located inside the detector gas volume and attached to a 0.25 cm thick aluminum window that acts as the replacement for the quartz window. The BaF_2 is a cylindrically shaped crystal, 7.6 cm in diameter and 1.27 cm thick, and is located at the entrance to the detector and replaces the quartz window.

3 The Fit to the Polya Distribution

In order to extract the number of detected photoelectrons produced by the crystal, two sets of data are recorded. The first set consists of a measurement of the single photoelectron spectrum using the hydrogen discharge lamp. The second set uses the radioactive source and one of the crystals, which we refer to as the multiple-photon spectrum. The shape of the single photoelectron spectrum is then used as input to the fit of the multiple-photon spectrum. The method used to fit the single photoelectron and multiple-photoelectron spectra is described in detail. A Monte Carlo procedure was used to test the accuracy of the fitting method.

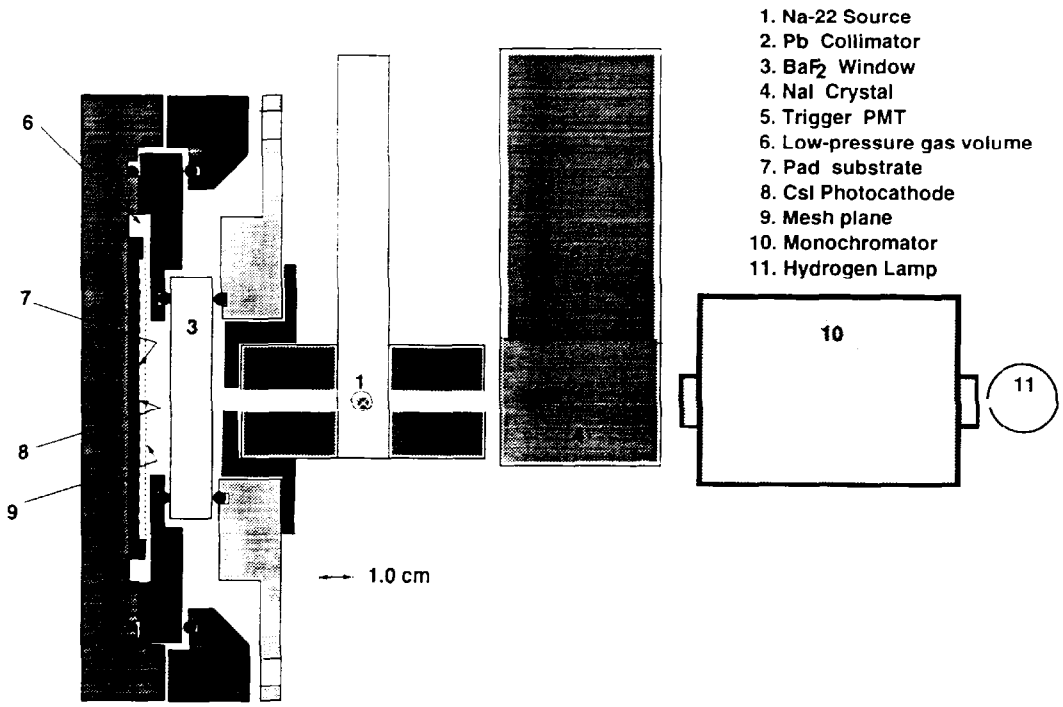

Figure 1: Schematic layout of the BaF_2 detector setup.

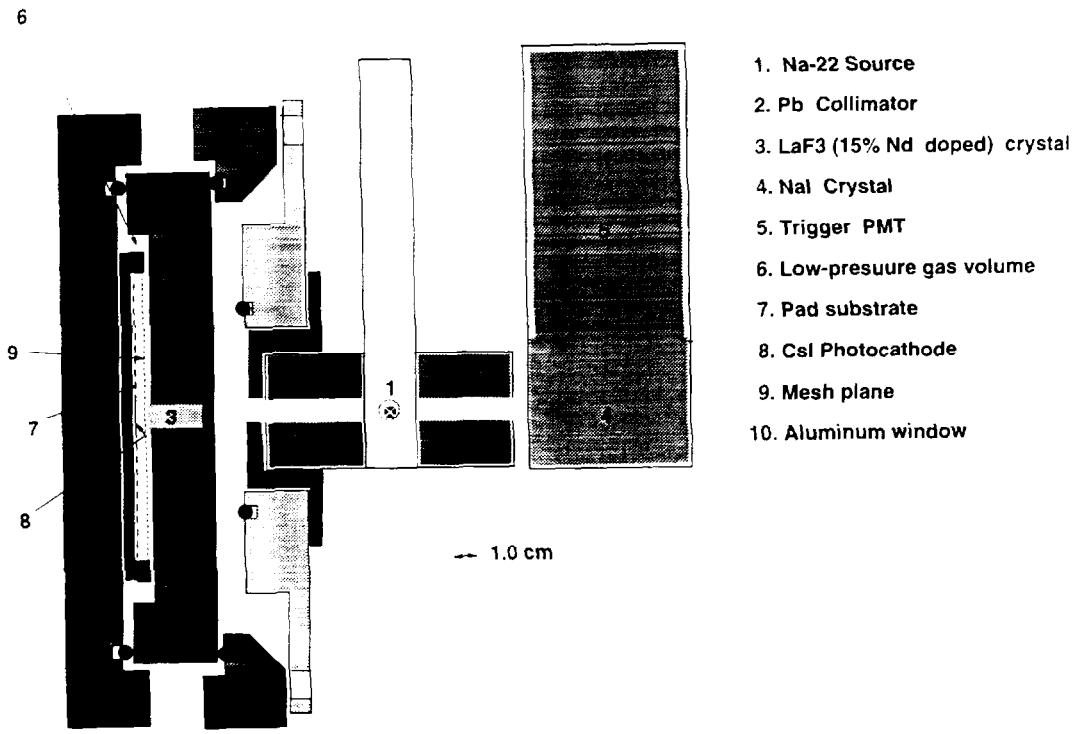

Figure 2: Schematic layout of the LaF_3:Nd^{3-} detector setup.

3.1 The Single-Photoelectron Fit

The single-photoelectron calibration data is dominated by events which have only one photon. This is guaranteed by cutting the mean photon rate per trigger to much less than 1.0. We fit the single-photoelectron calibration data to the sum of a Gaussian and a Polya distribution. The Gaussian represents those triggers that have no photon detected. The triggers that have one photon are modeled by a Polya distribution (the Polya distribution is usually referred to as the Gamma distribution in mathematical literature). This probability distribution is specified by:

$$f(x;b,c) = \frac{(bx/c)^b e^{-bx/c}}{x\Gamma(b)}$$

That is, the probability of getting a value in the infinitesimal range x to $x+dx$ from the Gamma distribution is $f(x;b,c)dx$. Note that the b parameter gives the power of x ($f(x;b,c) \propto x^{b-1}$), and the c parameter is the mean of the distribution. The standard deviation of the distribution is $c/\sqrt{b}$.

The procedure used is a binned maximum likelihood method. The first step in the procedure is to bin the data into about 800 bins. There are 6 variable parameters in the fit: 3 for the Gaussian and 3 for the Polya distribution. After several preliminary fits have brought the parameters close to their optimum values, the final fit adjusts the 6 parameters to maximize the likelihood function which characterizes the agreement between the data and the model. The likelihood function is based on the Poisson probability distribution that a particular bin will have the observed number of events. Explicitly, the likelihood is given by

$$\prod_i \frac{\mu_i^{n_i} e^{-\mu_i}}{n_i!}$$

where μ_i is the expected population of the ith bin (calculated from the 6 parameters) and n_i is the observed population of the ith bin. The main advantage of this method over other methods is that it handles bins with small populations correctly.

Figure 3 shows the result of a single-photoelectron fit to Monte Carlo data. The Monte Carlo data is generated using the exact mathematical distributions (in this case $\sim 50\%$ is a pure Gaussian and the rest is from a

pure Gamma distribution). The data is generated using the values $b = 3.1$ and $c = 300$, and the fit gives $b = 3.088 \pm 0.028$ and $c = 298.3 \pm 1.1$; the good agreement gives us confidence that the method is implemented correctly.

3.2 The Multiple-Photoelectron Fit

The Gamma distribution has the following property: n Gamma processes that independently contribute x (with probability $f(x; b, c)$) to a given measurement will when summed produce a new overall distribution specified by $f(x; nb, nc)$. In other words, the sum of n independent Gamma distributions is a Gamma distribution. The distribution for n photoelectrons ($n \geq 1$) is given by

$$f(x; nb, nc) = \frac{(bx/c)^{nb} e^{-bx/c}}{x\Gamma(nb)}$$

The model we use to fit our multiple-photoelectron spectrum is based on a Poisson probability of $\bar{n}^i e^{-\bar{n}}/i!$ for observing i photoelectrons, $\bar{n}$ being the mean number of photoelectrons observed. We still represent the zero-photoelectron piece by a Gaussian (3 variable parameters); the multiple photoelectron piece is proportional to

$$\sum_{i=1}^{\infty} \frac{\bar{n}^i e^{-\bar{n}}}{i!} f(x; ib, ic)$$

where the b and c are fixed at the values given by the single photoelectron fit, and 2 additional variable parameters ($\bar{n}$ and a normalization factor). Once again, the maximum likelihood fitting method is used.

Figure 4 shows the result of a multiple-photoelectron fit to Monte Carlo data. The data is generated using the values $b = 3.1$, $c = 300$ and $\bar{n} = 1.2$; the fit uses the results of the fit shown in Fig. 3 ($b = 3.088$ and $c = 298.3$) and finds $\bar{n} = 1.208 \pm 0.013$. This test increases our confidence that the multiple-photoelectron fit is implemented correctly.

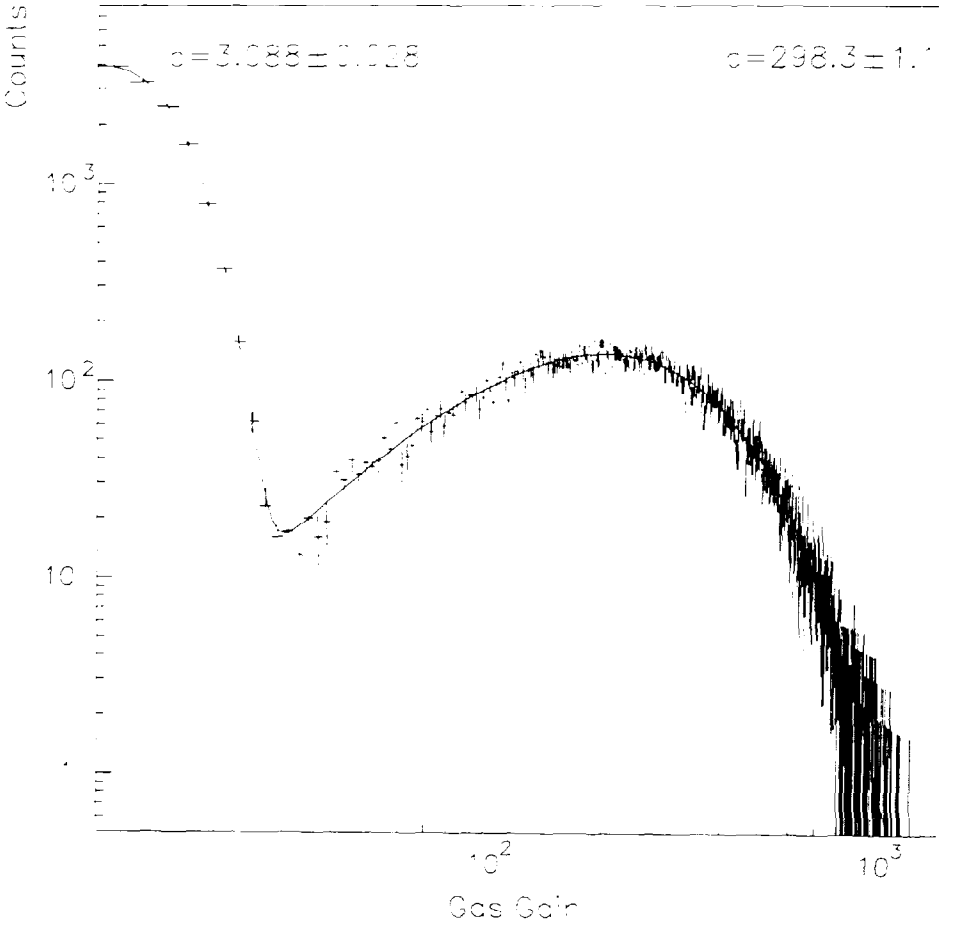

Figure 3: Fit of a Polya distribution (single photon) to Monte Carlo data. The Monte Carlo (single photon) is generated with $b = 3.1$ and $c = 300$. The values from the fit are $b = 3.088 \pm 0.028$ and $c = 298.3 \pm 1.1$. The horizontal bars indicate the bin size (not errors).

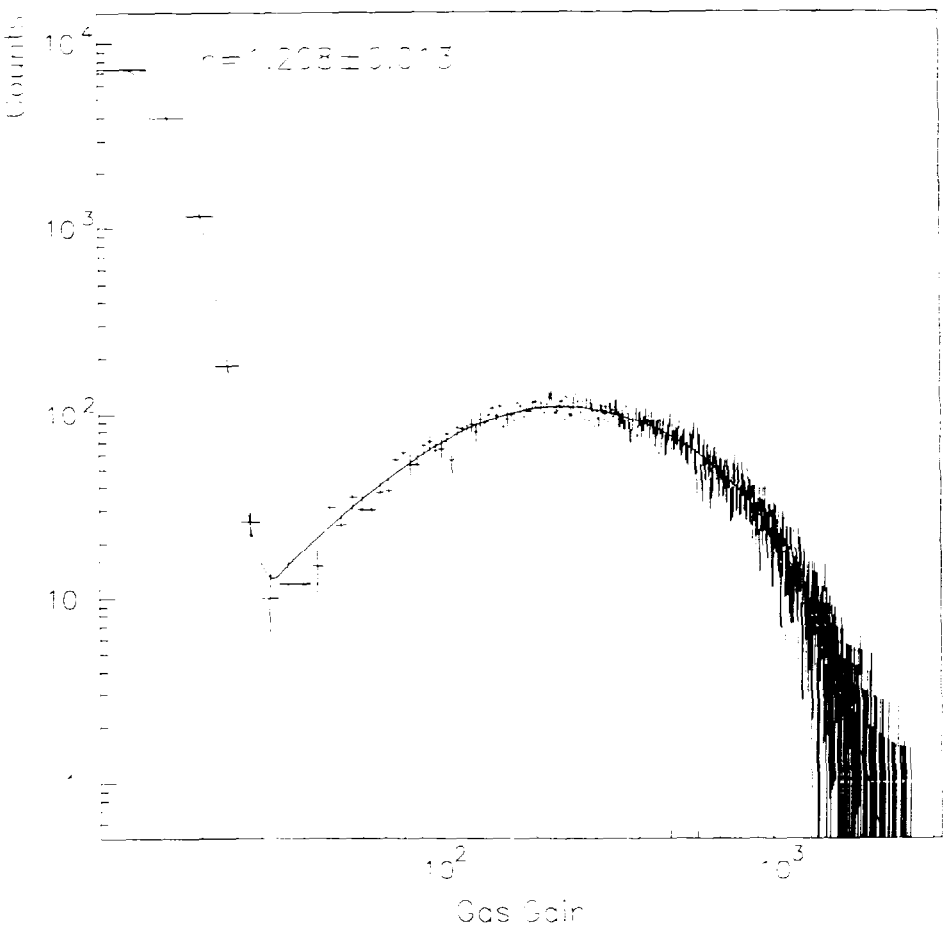

Figure 4: Fit of a multiple-Polya distribution to Monte Carlo data. The Monte Carlo (multi-photoelectron) is generated with $b = 3.1$, $c = 300$ and $\bar{n} = 1.2$. The value from the fit is $\bar{n} = 1.208 \pm 0.013$. The horizontal bars indicate the bin size (not errors).

3.3 Fitting the Multiple-Photoelectron Spectrum to a Polya Distribution

Using the Monte Carlo data described above, we fit a multiple-photoelectron spectrum to a single photoelectron distribution. Fig. 5 shows the Monte Carlo data of Fig. 4 (generated with $b = 3.1$, $c = 300$, and $\bar{n} = 1.2$) and an attempted fit to a single photoelectron distribution. We conclude that the fit quality is very poor and that the multiple-photoelectron distribution is poorly represented by any (single) Polya distribution.

4 Detector Simulation

In order to compare the measured results with expectations for the two types of crystals, the apparatus (Fig. 1 and Fig. 2) performance is evaluated with a Monte Carlo method simulation program. Positron-electron annihilations are modeled to occur within a three-dimensional Gaussian-weighted region at the geometric center of the source assembly. Positron production from the Na^{22} source and the 511 KeV gamma rays are isotropic. The collimator can completely absorb (photoelectric effect) or scatter the gamma ray. The scattering is modeled with the Compton effect, in which the gamma ray loses energy after the scatter. The gamma rays then enter the crystal, either BaF_2 or LaF_3:Nd^{3+}, and interact either with the Compton or photoelectric effect. The energy from the scattered electron is used to generate the number of photons.

Within the BaF_2 window, each photon is assigned a wavelength by the characteristic spectrum of which the fast component has peaks centered at 220 nm, 195 nm, and 175 nm and a total of 1400 photons/MeV are generated[9]. Energy loss can occur through two mechanisms. For 25% of the gamma ray interactions, the photoelectric effect is assumed to take place and the gamma ray energy is converted into UV photons. The remaining 75% of the gamma rays suffer Compton scattering, and the resultant scattered electron energy is converted into photons. Multiple Compton scattering is possible. This ratio is taken to be the same for both crystals. In addition, the NaI crystal is simulated as part of the trigger system. The number of photons generated from the LaF_3:Nd^{3+} crystal is 270 photons/MeV at 173 nm, as measured in Ref. [5].

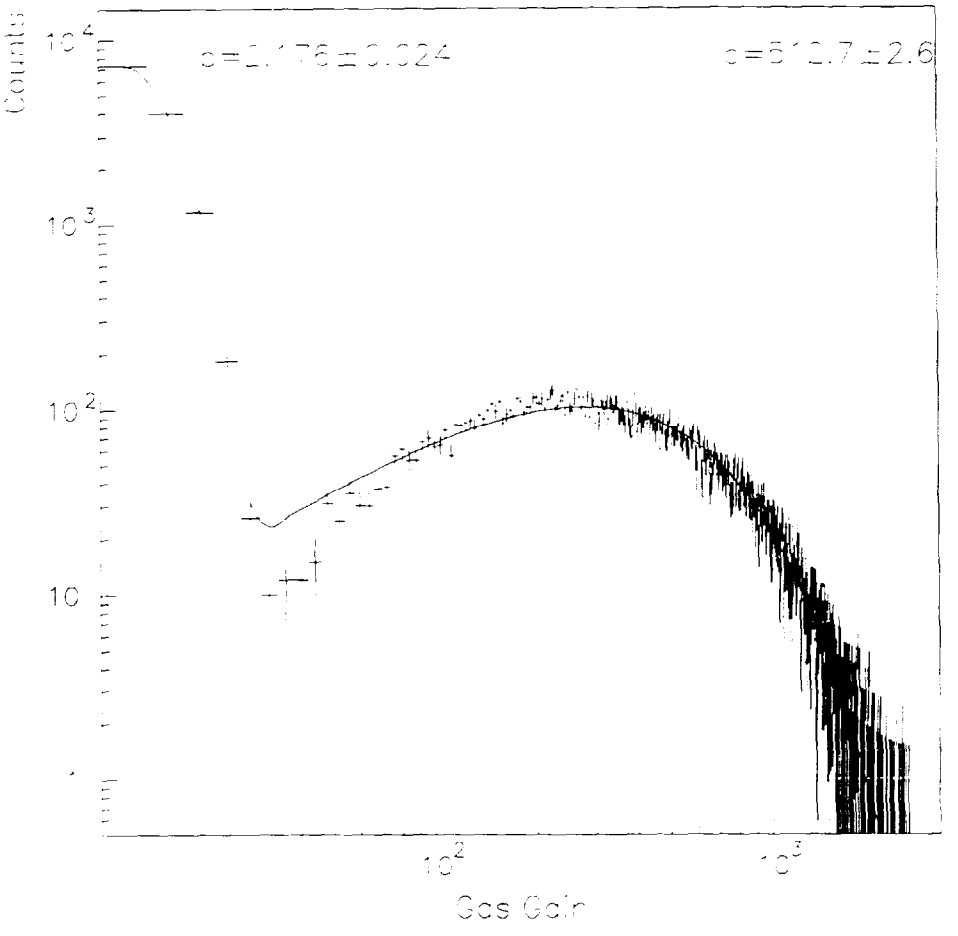

Figure 5: Fit of a single-photoelectron distribution to multiple-photoelectron Monte Carlo data. The Monte Carlo is generated with $b = 3.1$, $c = 300$ and $\bar{n} = 1.2$. The poor quality of the fit reflects the fact that the generated and fitted distributions are of a different form. The horizontal bars indicate the bin size (not errors).

The simulation program traces the paths of the photons inside the crystal until they impinge on the CsI photocathode or until they are lost. The three relevant surfaces of the crystal cylinder are the: 1) front face 2) rear face and 3) the cylindrical wall. Reflection from the front face is specular and the amount of reflection or transmission is calculated from the indices of refraction of the two media and the angle of incidence of the ray (Fresnel coefficients). The transmission angles are calculated using Snell's Law. The indices of refraction of the LaF_3:Nd^{3+} and BaF_2 crystals are $n = 1.70$ and $n = 1.56$ respectively. We use $n = 1.0$ for the low pressure ethane in the chamber. No absorption loss of the UV photons is modeled in the crystals.

Reflection from the rear face is specular, the amount of reflection and transmission being determined by the Fresnel coefficients. The transmitted photons impinge on a white diffuse reflector (teflon, 95% efficient) and then reenter the crystal at a random angle. Reflection from the wall's surface is treated in the same manner as the rear face.

The $\sim$ 80% transmission at normal incidence of the steel mesh and the CsI quantum efficiency, which ranges from 22% at 170 nm to 4% at 200 nm, is included in the model based on measurements from Ref. [3]. The geometry of the collimator, window and PPAC are all modeled.

The results of the simulation are summarized in Table 1. The overall efficiency for detecting the photons produced in both crystals is small, about 2% for the LaF_3:Nd^{3+} and 0.4% for the BaF_2. The expected detected number of photoelectrons after all efficiencies from both crystals is ~ 5.

We find the CsI quantum efficiency to be the largest source of loss in the system. A further important inefficiency is the total internal reflection from the front face of the crystal. This large inefficiency results from the poor matching of indices of refraction between the crystal and the low pressure gas volume. The steel mesh accounts for an additional loss and finally a small loss occurs due to the finite size of the central active pads. The results for these losses are summarized in Table 2.

Table 1: Detector Simulation Results

Physics Process	BaF_2	LaF_3:Nd^{3+}
$e^-e^- \rightarrow \gamma\gamma$ generated	10^7	10^7
γ rays depositing energy	6428	5901
UV-photons generated	2.6×10^6	4.5×10^5
Mean Energy deposited	0.31 MeV	0.31 MeV
No. of photoelectrons after losses	11002	10343
Events with ≥ 1 photoelectrons	4349	4259
Photoelectrons/MeV	5	5

Table 2: Summary of Average Losses from the Detector Simulation.

Cause of Loss	BaF_2-Efficiency	LaF_3:Nd^{3+}-Efficiency
Steel Mesh	0.80	0.80
Geometry between pad and crystal	0.80	0.95
CsI Quantum efficiency	0.055	0.2
sides and rear face of crystal	0.6	0.4
crystal-ethane interface (front face)	0.2	0.36
Total efficiency	0.004	0.022

5 Results

5.1 Results for the BaF_2

The data for the single photoelectron spectrum calibration using the hydrogen discharge lamp are shown in Fig. 6. The monochromator selects 180 nm for this measurement. The fit to the Polya distribution is very good. The parameters b and c, determined from the fit, are then used as inputs to the multiple-photoelectron fit. Shown in Fig. 7 are the data from the 511 KeV gamma ray source incident on the BaF_2 window. The result gives a mean number of photoelectrons of $\bar{n} = 0.91 \pm 0.01$. We then correct $\bar{n}$ for the effects of the loss of transmission through the mesh, (80% transmission at normal incidence), and a mean energy deposited of 60%. Our final result is 3.71 ± 0.04/MeV, where the error is statistical.

5.2 Results LaF_3:Nd^{3+}

Shown in Fig. 8 are the data from the 511 KeV gamma ray source incident on the LaF_3:Nd^{3+} crystal. The result gives a mean number of photoelectrons of $\bar{n} = 1.18 \pm 0.01$. We then correct $\bar{n}$ for the effects of the loss of transmission through the mesh, (80% transmission at normal incidence), and mean energy deposited of 60%. Our final result is 4.81 ± 0.04/MeV, where the error is statistical. The 10 mol% and 15 mol% doped samples gave the largest signal and are essentially the same within the stated errors. The results reported are for the 15 mol% doped crystal.

5.3 Systematics

The main systematic error comes from the uncertainty in the quantum efficiency for the photocathode. We have estimated this uncertainty in previous work [3] to be 20%. There is a systematic uncertainty associated with the modeling of the correction due to Compton energy loss that we estimate to be 10%. The uncertainty in the Compton correction factor arises from a lack of knowledge for the ratio of Compton scattering to photoelectric effect, which we take to be 3:1. We include an additional uncertainty 20% due to the poor fit of the multi-photoelectron data to the model. We combine these in quadrature for a total systematic error of 30%.

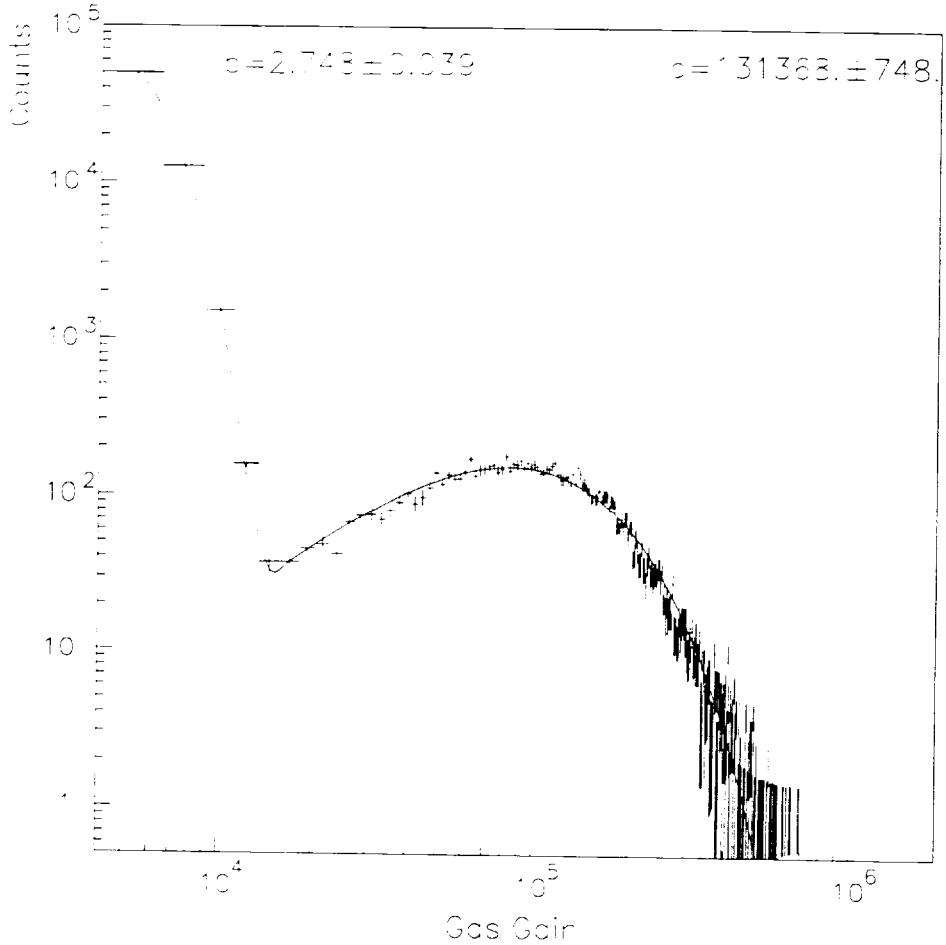

Figure 6: Plot of the single photoelectron spectrum plus background fit with Polya distribution and a Gaussian.

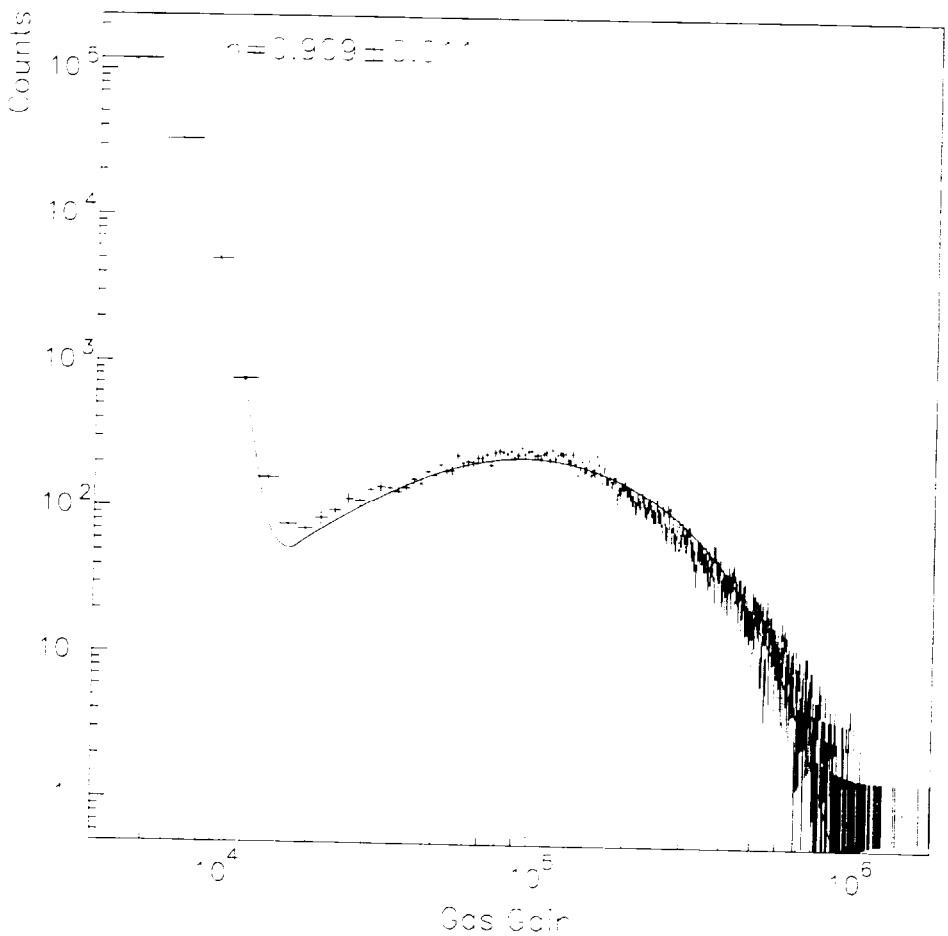

Figure 7: Plot of the photoelectron spectrum plus background from BaF_2 fit with the multiple-photoelectron Polya distribution and a Gaussian.

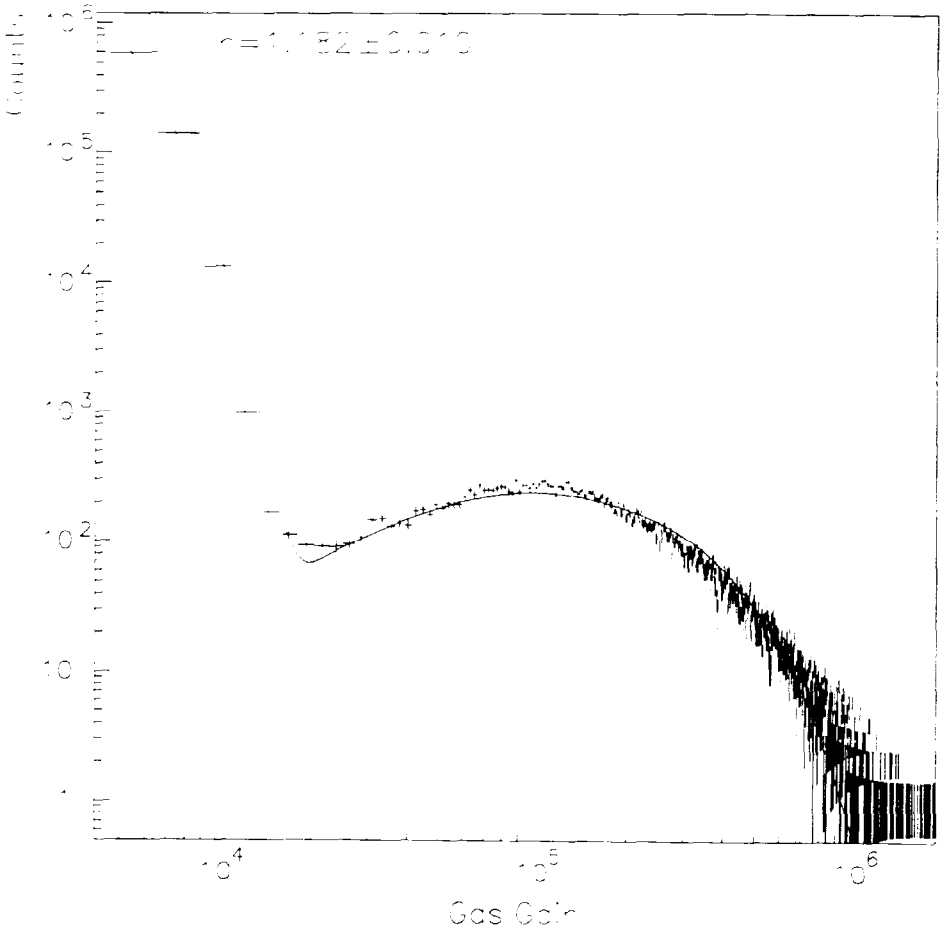

Figure 8: Plot of the photoelectron spectrum plus background from LaF_3:Nd^{3+} fit with the multiple-photoelectron Polya distribution and a Gaussian.

6 Conclusion

We have measured the number of detected photoelectrons in the sensitive range for a CsI photocathode, when an incident gamma ray of energy 511 KeV is incident on two different crystals. We find $3.71 \pm 0.04 \pm 1.11$ photoelectrons per MeV for the BaF_2 crystal and $4.81 \pm 0.04 \pm 1.44$ photoelectrons per MeV for the LaF_3:Nd^{3+} crystal. As indicated in ref. [5], we expect 270 photons/MeV at 173 nm. Using a detailed Monte Carlo simulation of the detector and physics processes we estimate 5 photoelectrons/MeV should be detected for both crystals. We note the 1400 photons/MeV in BaF_2 relative to 270 photons/MeV in LaF_3:Nd^{3+} essentially offsets with the lower quantum efficiency of CsI at the peak of the BaF_2 emission relative to the higher quantum efficiency at the LaF_3:Nd^{3+} emission peak of 173 nm.

Our simulations indicate that the photon yield could be improved by almost a factor of three by using a semi-transparent photocathode in contact with the crystal rather than the reflective photocathode used in this test [10].

References

[1] D. Anderson *et al.*, Nucl. Instr. and Meth. A 326 (1993) 611.

[2] N. S. Lockyer *et al.*, Nucl. Instr. and Meth. A 332 (1993) 143.

[3] W. Kononenko and N. S. Lockyer, Nucl. Instr. and Meth. A 371 (1996) 143.

[4] A. Braem *et al.*, Nucl. Instr. and Meth. A 343 (1994) 163.

[5] P. Dorenbos *et al.*, *The Intensity of the 173 nm emission of* LaF_3*:*Nd^{3+} Submitted to Nucl. Instr. and Meth. (1996).

[6] P. Schotanus *et al.*, Nucl. Instr. and Meth. A 272 (1988) 913.

[7] P. Schotanus *et al.*, Nucl. Instr. and Meth. A 284 (1989) 531.

[8] M. Gruwe and S. Taviernier *et al.*, Nucl. Instr. and Meth. A 311 (1992) 301.

[9] P. Dorenbos *et al.*, IEEE Trans. Nucl. Sci. 40, (1993) 424.

[10] C. Lu and K. T. McDonald, Nucl. Instr. and Meth. A 343 (1994) 135.